Electronic Supplementary Information (ESI†)

PVDF/Ag_2CO_3 Nanocomposites for Efficient Dye Degradation and Flexible Piezoelectric Mechanical Energy Harvester

Hari Krishna Mishra[a], Dipanjan Sengupta[a], Anand Babu[a], Bilal Masood Pirzada[b, ‡], Ranjini Sarkar[c], Boddu S. Naidu[b], Tarun Kumar Kundu[c] and Dipankar Mandal[a, *]

[a]*Department of Quantum Materials and Devices, Institute of Nano Science and Technology, Knowledge City, Sector-81, Mohali 140306, India*

[b]*Department of Energy and Environment, Institute of Nano Science and Technology, Knowledge City, Sector-81, Mohali 140306, India*

[c]*Department of Metallurgical and Materials Engineering, Indian Institute of Technology Kharagpur, Kharagpur, West Bengal 721302, India*

[‡]*Present address: Department of Chemistry, Khalifa University of Science and Technology, Abu Dhabi 127788, United Arab Emirates*

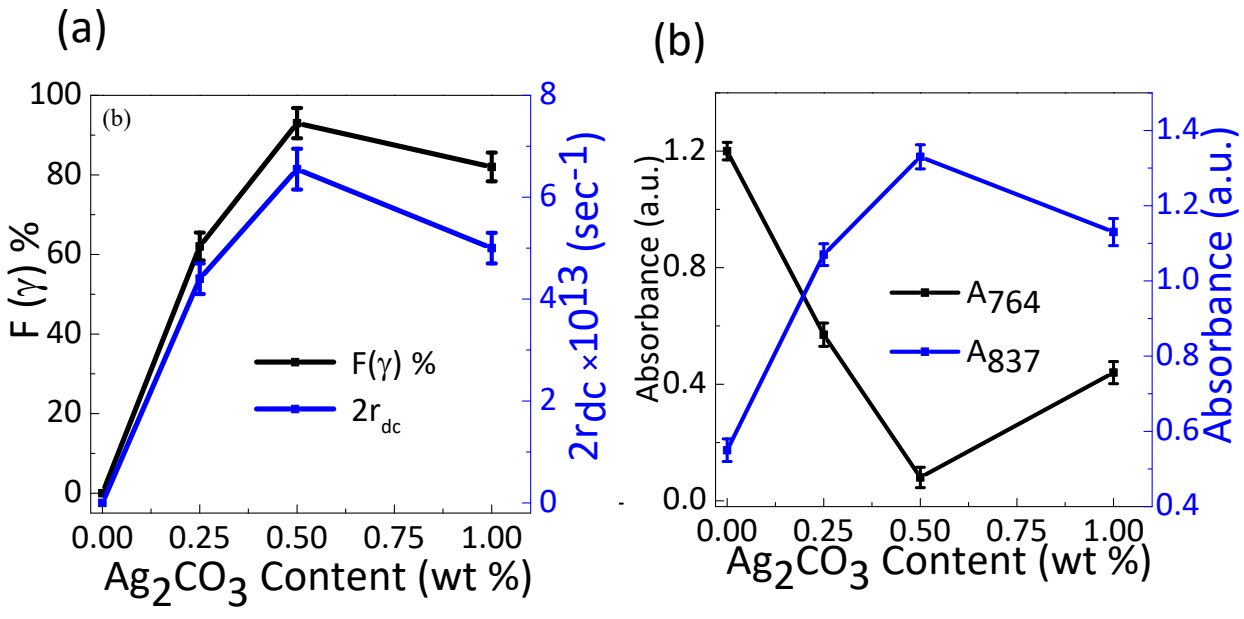

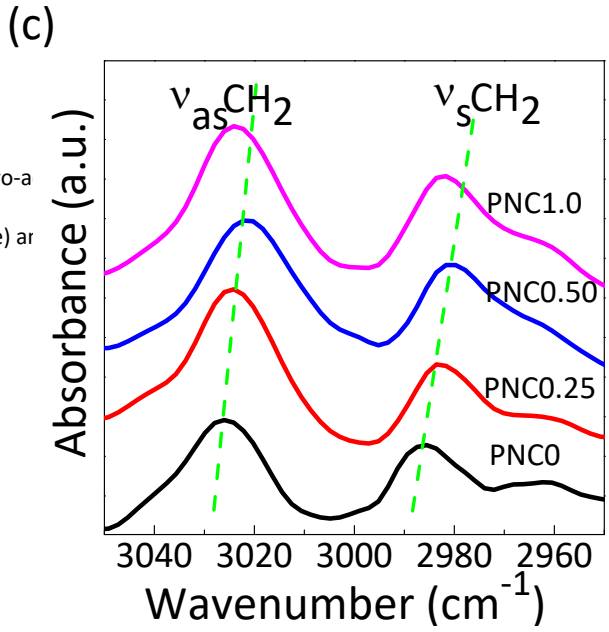

Fig. S1 (a) Variation of electro-a or variation in PNC film, (b) Intensity variation of 837 (for γ-phase) ar ; in PNC films.

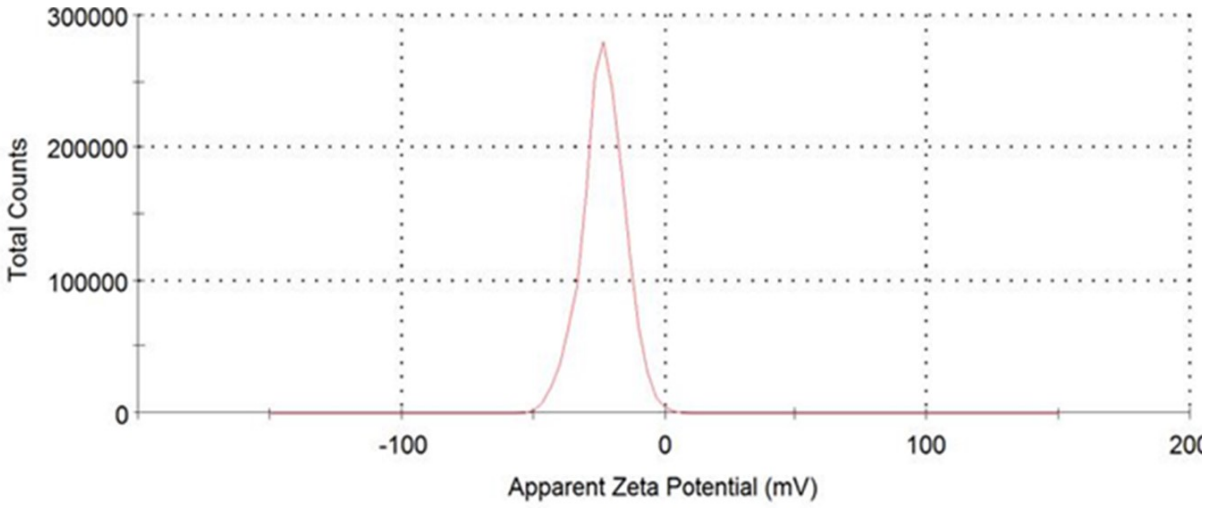

Fig. S2 Zeta (ζ) potential distribution (-23.2 mV ± 0.462) of Ag_2CO_3 nanorods.

Associated discussion S1: Decomposition Ag_2CO_3 into Ag Nanoparticles (Ag NPs)

It can be experimentally proven by X-ray photoelectron spectroscopy (XPS) spectra as shown in Fig. S3. To a better understanding, we have considered two cases 1) as-synthesized Ag_2CO_3, and 2) heat-treated Ag_2CO_3 at 120 °C for 8 h as used for the composite film preparation. Then we have collected the XPS spectra for both cases as shown in Fig. S3. It can be observed from Ag spectra that two peaks are present $Ag3d_{5/2}$ and $Ag3d_{3/2}$ at peak positions 367.3 and 373.3 eV respectively due to the presence of silver carbonate (Ag_2CO_3) and there are no other shoulder peaks present as shown in Fig. S3a. While in the case of heat-treated Ag_2CO_3 there are two peaks present at the same peak positions 367.3 and 373.3 eV respectively which is for Ag_2CO_3 but two more small peaks are observed at the peak position of 368.4 and 374.4 eV respectively which is associated with the silver nanoparticles (Ag NPs) as shown in Fig. S3b. These results are well agreed with the literature.[1,2] Thus, we can say that the prolonged stay of Ag_2CO_3 in the PVDF matrix at 120 °C may decompose Ag_2CO_3 into Ag NPs to some extent.

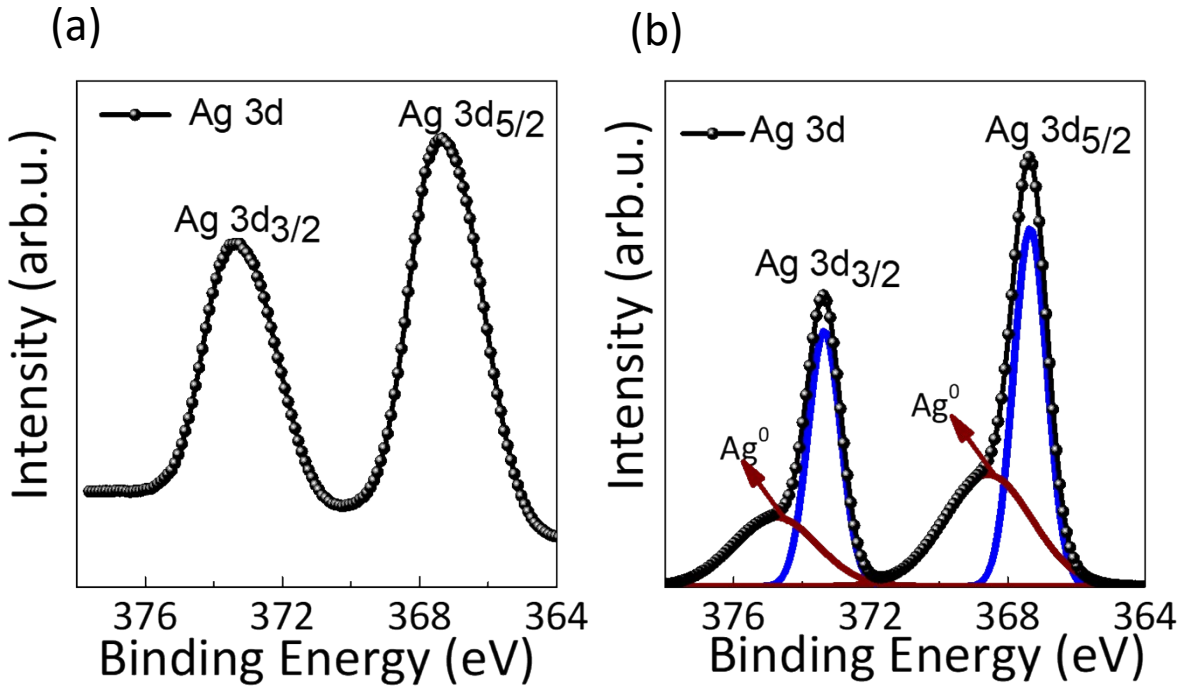

Fig. S3. The high-resolution Ag3d XPS spectra of (a) as-synthesized and (b) after heat-treated Ag2CO3 at 120 °C (This temperature is selected in order to follow the PVDF/Ag2CO3 nanocomposite film preparation).

Associated discussion S2: Computational details of DFT

The intermolecular interactions between PVDF and silver carbonate fillers (Ag_2CO_3) are explored by density functional theory (DFT) calculations based on linear combination of atomic orbitals (LCAO) approach. Geometry optimization and frequency calculations are carried out for isolated α-, β-, and γ-PVDF tetramers, Ag_2CO_3 molecule, and PVDF/ Ag_2CO_3 systems in Gaussian16 suite of programs. Grimme's dispersion-correction (DFT-D3) is implemented on standard exchange-correlation functional B3LYP.[3] Triple zeta basis set 6-311+G(d,p) are used for C, H, and O atoms, and effective core potential (ECP) basis set LANL2DZ is used for Ag atoms.[4] Solvation model calculations are performed considering DMF solvent (ε=37.219) using integral equation formalism polarizable continuum model (IEFPCM).[5] Atomic dipole moment corrected Hirshfeld charge (ADCH) population[6] and Bader's quantum theory of atoms in molecules (QTAIM)[7] analyses analysis is performed using multi wavefunction analyser Multiwfn code.[8]

Solvation energy $(\Delta E)_{sol}$ of a system under study has been calculated as,

$$(\Delta E)_{sol} = E_{sol} - E_{gas} \quad (1)$$

E_{gas} and E_{sol} are the zero-point error (ZPE) and basis set superposition error (BSSE) corrected energies of the system in the gas phase and in DMF, respectively. BSSE calculations are performed based on the counterpoise method.[9] Negative solvation energies (Table S1, ESI†) indicate solution phase stability of the systems.

Binding energies of PVDF/filler (Ag_2CO_3) complexes are calculated as,

$$\Delta E_{bind} = E_{PVDF/filler} - (E_{PVDF} + E_{filler}) \quad (2)$$

$E_{PVDF/filler}$, E_{PVDF} and E_{filler} are the ZPE and BSSE corrected total electronic energies of the separately optimized structures of PVDF/filler complex, PVDF tetramers (α, β, and γ phases) and the filler Ag_2CO_3, respectively. For gas phase and solvation model calculations, these energy values correspond to the energies of the gas phase and solution phase geometries of the systems, respectively.

Table S1. Solvation energies, dipole moments, binding energies, and partial charges of PVDF fragments within PVDF/Ag_2CO_3 complexes in DMF.

PVDF/filler complexes	Solvation energy (kcal/mol)	Dipole moment (D) in DMF	Binding energy (kcal/mol) in DMF	Partial charge of the PVDF fragment in DMF
α-PVDF/Ag_2CO_3	-39.97	9.56	-3.01	-0.058
β-PVDF/Ag_2CO_3	-37.85	4.76	-9.93	0.007
γ-PVDF/Ag_2CO_3	-35.88	7.60	-10.22	-0.042

The regions of γ-PVDF/Ag_2CO_3 non-covalent interactions (Ag…F and O…H) are determined from the bond path analysis based on Bader's QTAIM. Electron density (ρ) and Laplacian of electron density $(\nabla^2\rho)$ at the bond critical points (BCPs) are given in Table S2. The non-covalent bonds are identified by the positive values of $\nabla^2\rho$ at the corresponding BCPs. The strength of similar types of non-covalent bonds are compared by the bond lengths and corresponding ρ values (Table S2, ESI†). A stronger bond exhibits a lower bond length and higher ρ.

Table S2. Ag…O and O…H non-covalent bond lengths and corresponding electron density (ρ) and Laplacian of electron density ($\nabla^2\rho$) values at the BCPs.

Non-covalent bonds	Bond lengths (Å)	ρ (a.u)	$\nabla^2\rho$ (a.u)
Ag31…F8	3.12	0.0072	0.0286
Ag31…F22	2.99	0.0098	0.0388
Ag32…F25	2.89	0.0116	0.0489
Ag32…F23	3.38	0.0045	0.0168
O28…H16	2.17	0.0173	0.0577
O30…H5	2.23	0.0154	0.0487

Associated discussion S3: XPS analysis of PNC film

The interaction between PVDF and Ag_2CO_3 has been further confirmed by surface analysis from XPS. We have collected the spectra for PNC0 and PNC0.50 film as shown in Fig. S4. In Fig. S4a, we can observe the Ag spectra from PNC0.50 film and respective peaks positions at 368.1 and 374.2 eV resembles the interaction between PVDF and Ag_2CO_3 due to little shift in the peak position of Ag_2CO_3 (as shown in Fig S3a). Next, O 1s spectra also show the interaction between PVDF and Ag_2CO_3 with positions associated with 531 eV as shown in Fig. S4b. The C1s and F1s exhibit the exclusive interactions between PVDF and Ag_2CO_3 with respect to PNC0 because in the PNC0.50 film -CH_2- and -CF_2- region are little shifted towards higher binding energy and similar nature is found from F1s spectra as shown in Fig. S4c and S4d respectively.

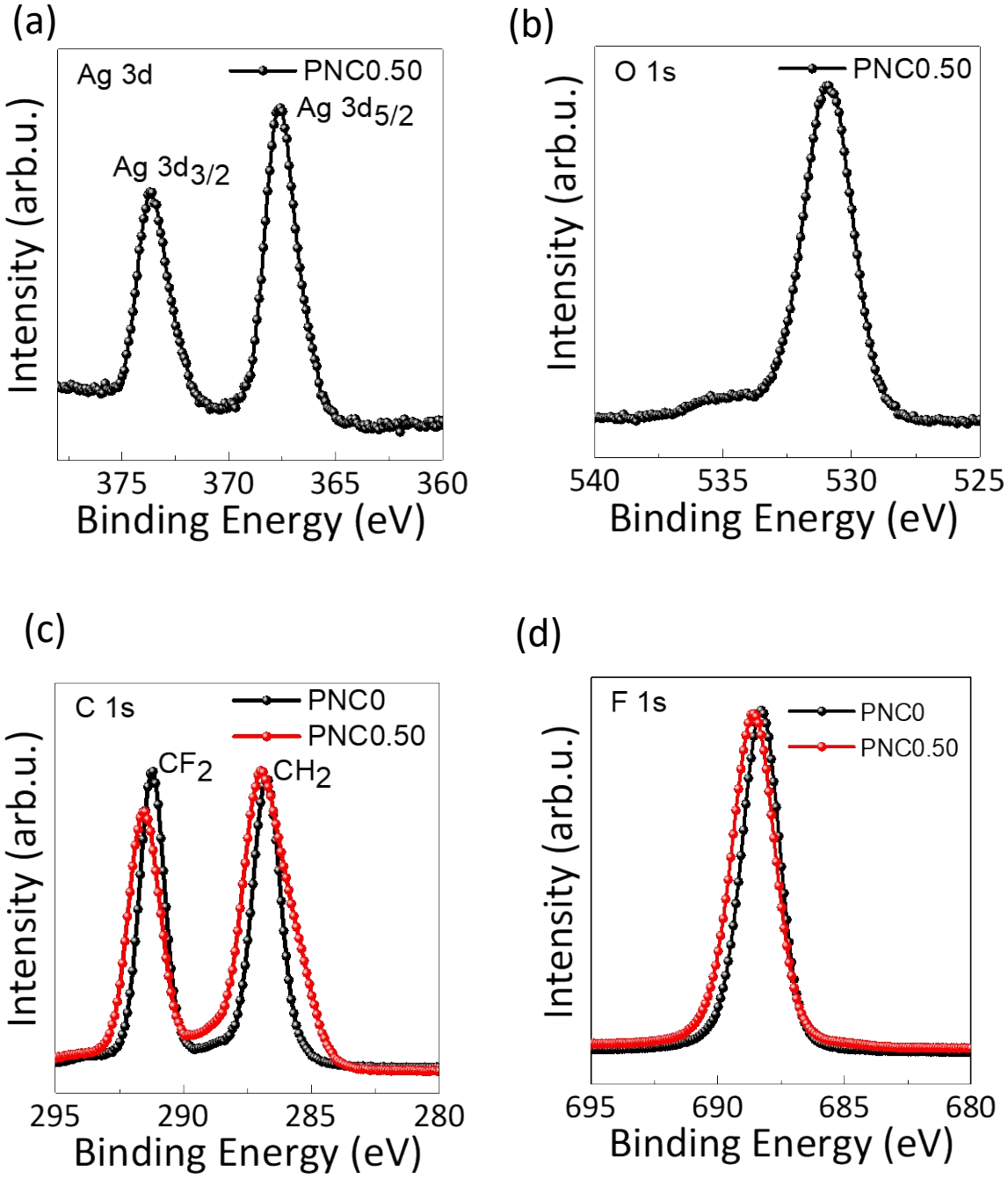

Fig. S4. The high resolution XPS spectra of (a) Ag3d, (b) O1s of PNC0.5 film, (c) C1s and (d) F1s XPS spectra of PNC0 and PNC0.50 film.

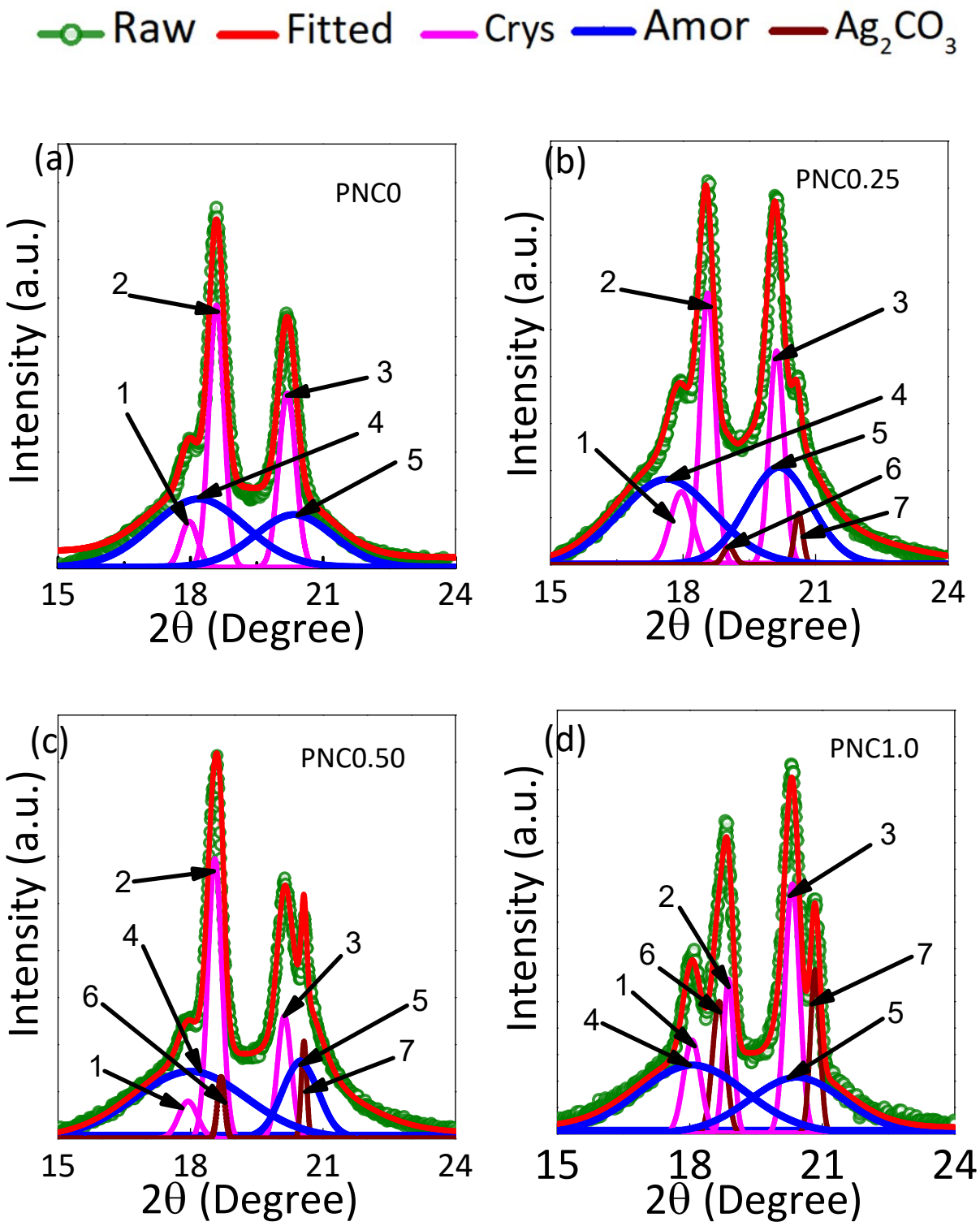

Fig. S5. The curve deconvolution of XRD pattern of (a) PNC0 (b) PNC0.25, (c) PNC0.50 and (d) PNC1.0. In PNC0 the peaks marked as 1, 2 and 3 are the crystalline peaks having reflection plane (100), (020) and (110) respectively which indicates the characteristics peaks of α-phase of PVDF. Two broad hallows (4, 5) shows amorphous region. In the PNC films, the peaks marked as 1, 2 and 3

representing the crystallne region with reflection planes (100), (020) and (110) respectively, and the marked peak 4, 5 are due to amorphous region of PNC films. The peaks marked as 6, 7 with reflection plane (020) and (110) are showing the presence of Ag_2CO_3 into PVDF matrix. The intensity of peaks 6, 7 increases as the filler (Ag_2CO_3) concentration increases into the PVDF matrix. The crystallinity (%) are estmated by considereing the area of crystalline and amorphous part which is listed in the Table S3.

Table S3: The degree of crystallinity estimated from deconvoluted XRD pattern.

Sample	Crystallinity (%)
PNC0	51
PNC0.25	47
PNC0.50	40
PNC1.0	42

(a)

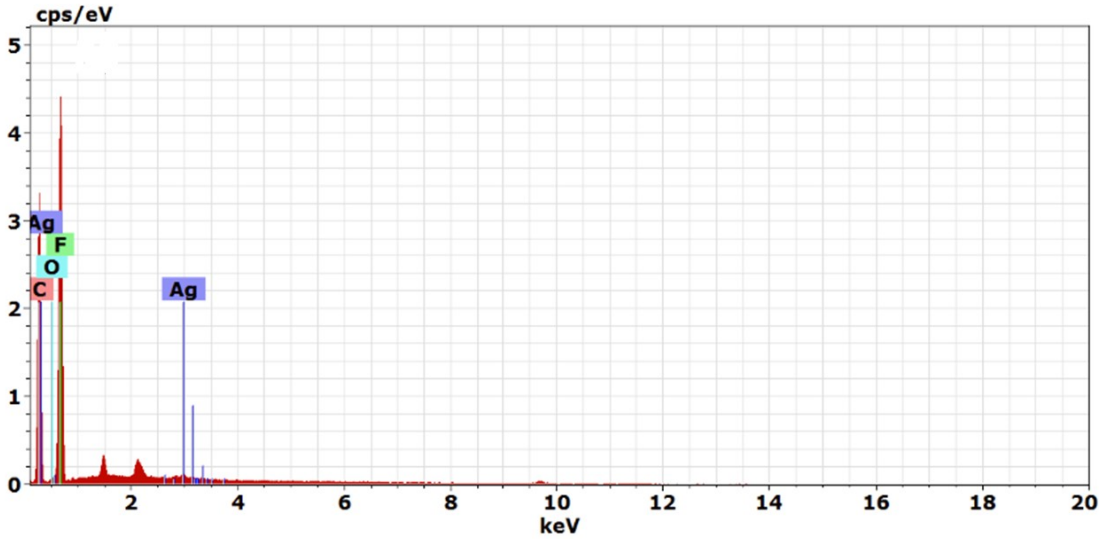

(b)

Element	series	[wt.%]	[norm. wt.%]	[norm. at.%]	Error in wt.% (3 Sigma)
Carbon	K-series	49.75651	49.75651	61.1857	18.71042
Fluorine	K-series	48.67635	48.67635	37.84253	17.47905
Silver	L-series	0.604083	0.604083	0.082715	0.164488
Oxygen	K-series	0.96306	0.96306	0.889055	0.939995
	Sum:	100	100	100	

(c)

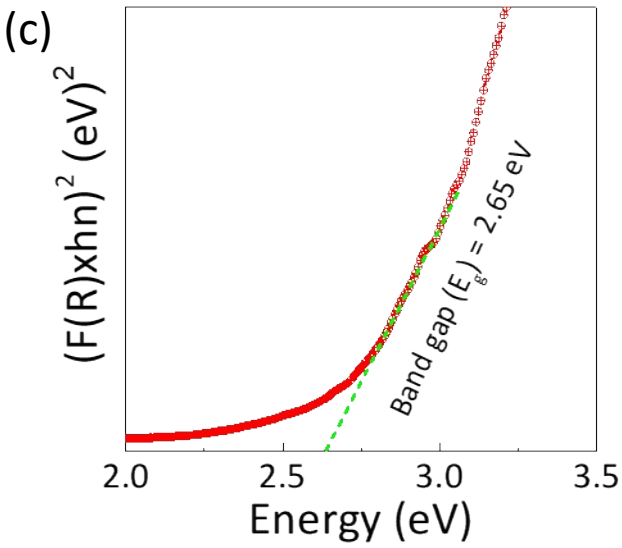

Fig. S6. (a) EDX mapping, (b) elemental quantification of PNC0.50 film and (c) energy band gap (E_g) of as synthesized Ag_2CO_3 nanorods.

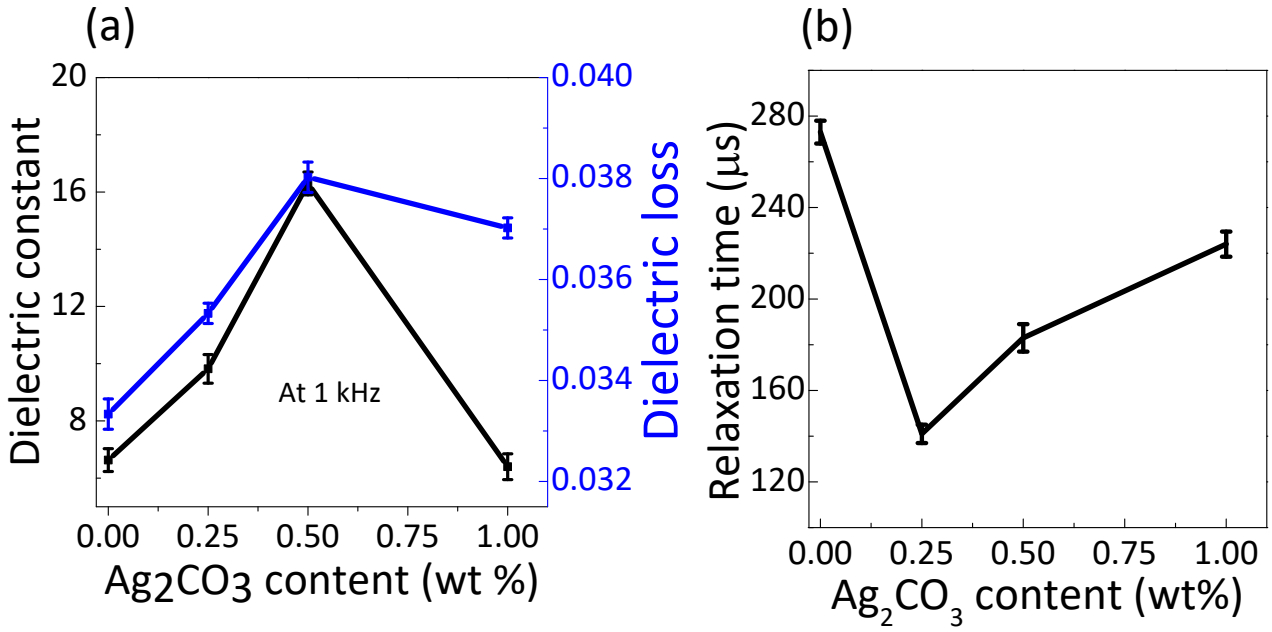
(a)
Dielectric constant
Dielectric loss
At 1 kHz
Ag2CO3 content (wt %)
(b)
Relaxation time (μs)
Ag2CO3 content (wt%)

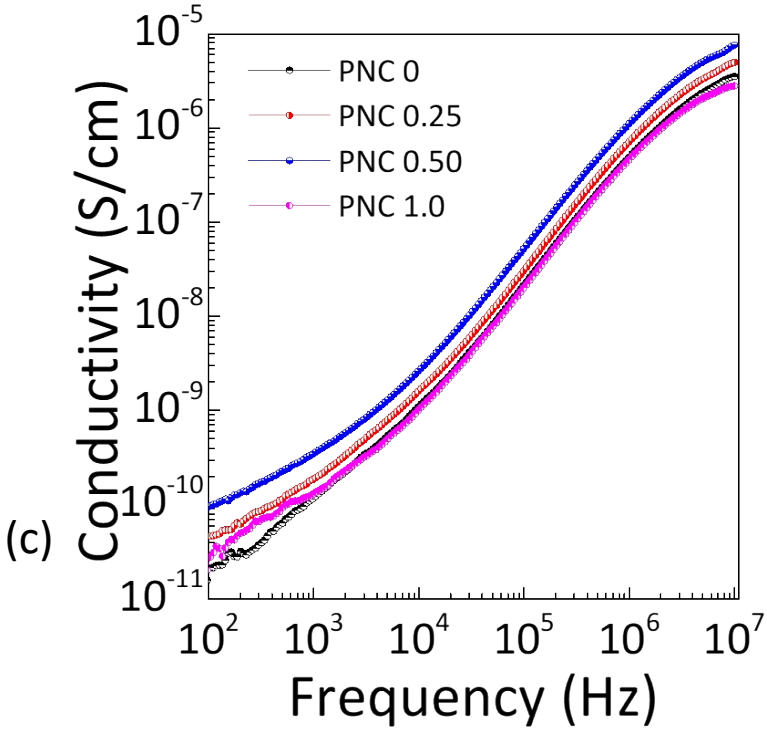
(c)
Conductivity (S/cm)
PNC 0
PNC 0.25
PNC 0.50
PNC 1.0
Frequency (Hz)

Fig.S7. Dependance of (a) dielectric constant and loss tangent 1 kHz frequency, (b) the relaxation time of PNC films corresponding to the frequency of lowest dielectric loss and (c) AC conductivity at room temperature with the incorporation of different wt % of Ag_2CO_3 nanorods into PVDF matrix.

Associated discussion S4: Calculation of pressures for mechano-sensitivity

Force was calculated based on two laws of classical physics namely, kinetic energy theorem and momentum conservation law respectively. In this context, we used free falling object (here used weight box of different mass) under the gravitational acceleration ($g = 9.8\ {}^{m}/_{s^2}$) on the PNG device. When the object falls on the device then two phenomenon happening 1) Object comes from a constant height with an initial velocity and just touches the surface of the PNG device, 2) Object completely acting on the PNG device (during the complete contact of object to the device the final velocity is almost zero since object is in rest for a very short time). In second case the force (impulse force) is acting for a very short time ($\Delta t = 10\ ms$). Now, based on the following equation force can be calculated

$$mgh = \frac{1}{2}mv^2 \quad \text{S1}$$

$$(F - mg)\Delta t = mv \quad \text{S2}$$

where, m is the mass of the objects falling to the device surface and h is the constant height from where object falls, v is the velocity by which object touches the device and F is the axial force.

Furthermore, the pressure was estimated as

$$\sigma_a = {}^{F}/_{A} \quad \text{S3}$$

where, A is the effective area of during force imparting.

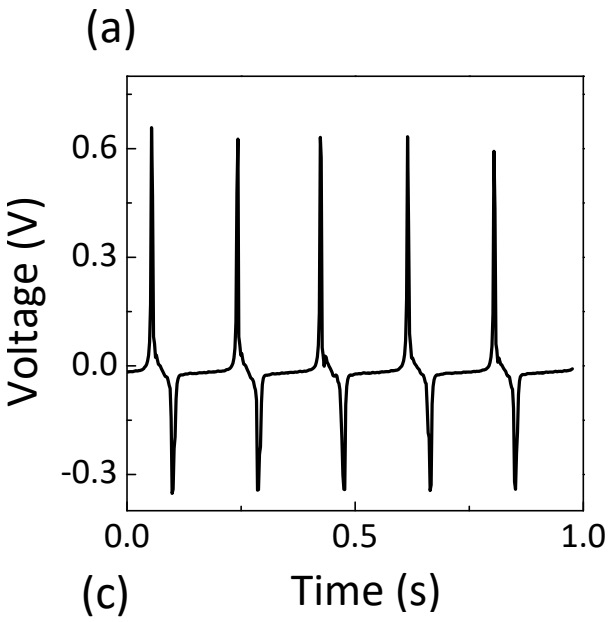
(a)
Voltage (V)
0.6
0.3
0.0
-0.3
0.0
0.5
1.0
Time (s)

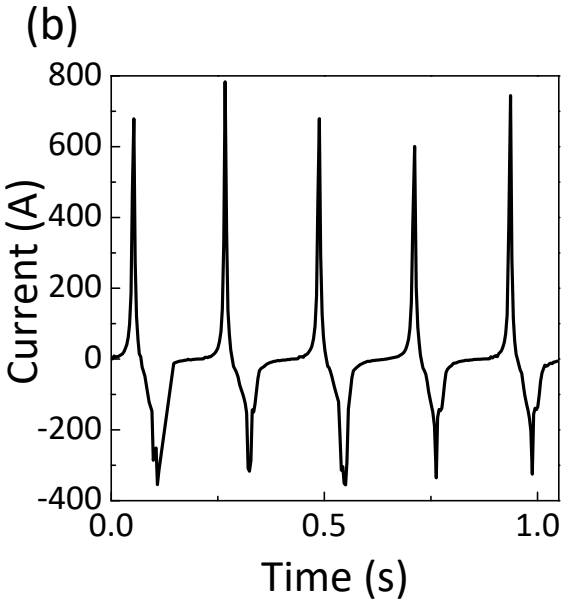
(b)
Current (A)
800
600
400
200
0
-200
-400
0.0
0.5
1.0
Time (s)

(c)


AUX
FPNG

Fig. S8. (a) the open circuit voltage of control device, (b) short circuit current of the control device and (c) set-up (FPNG placed on the front of speaker)) for acoustic measurements.

Table: S4 Performance of piezoelectric nanogenerator with different processing conditions.

Materials	Method of Preparation	Open circuit voltage (V)	Short circuit current (μA)	Power density (μW/cm^2)	References
$BaTi_{(1-x)}Zr_xO_3$/PVDF	Solution casting	11.9	1.35	0.14	10
Ag-pBT/PVDF	SLS technique	10	0.14	-	11
ZnO/PVDF	Solution casting	11	9.8	0.44	12
Polydopamine/$BaTiO_3$/P(VDF-TrFE)	Electrospinning	6	1.5	0.85	13
PMN-PT/PVDF	Tape casting	10.3	0.04	-	14
Graphene/PVDF	Electrospinning	7.9	4.5	-	15
Ag-$BaTiO_3$/PVDF	Solution casting	14	0.96	0.98	16
$MAPbBr_3$/PVDF	Electrospinning	5	0.06	0.28	17
$NaNbO_3$/PVDF	Solution casting	3.34	0.53	-	18
Tri-layer of BTO/PVDF	Spin coating	10	2.5	0.72	19
Ag_2CO_3/PVDF	Solution casting	15	6	7	this work

References:

1 G. B. Hoflund, Z. F. Hazos and G. N. Salaita, *Phys. Rev. B - Condens. Matter Mater. Phys.*, 2000, **62**, 11126–11133.

2 J. F. Weaver and G. B. Hoflund, *Chem. Mater.*, 1994, **6**, 1693–1699.

3 S. Grimme, J. Antony, S. Ehrlich and H. Krieg, J. Chem. Phys., 2010, **132**, 154104.

4 P. J. Hay and W. R. Wadt, J. Chem. Phys., 1985, **82**, 270–283.

5 G. Scalmani and M. J. Frisch, J. Chem. Phys., 2010, **132**, 114110.

6 T. Lu and F. Chen, J. Theor. Comput. Chem., 2012, **11**, 163–183.

7 P.S.V. Kumar, V. Raghavendra, V. Subramanian, J. Chem. Sci., 2016, **128**, 1527–1536.

8 T. Lu and F. Chen, Journal of Computational Chemistry, 2012, **33**, 580–592.

9 F. B. van Duijneveldt, J. G. C. M. van Duijneveldt-van de Rijdt and J. H. van Lenthe, Chem. Rev., 1994, 94, 1873–1885

10 N. R. Alluri, B. Saravanakumar and S. J. Kim, ACS Appl. Mater. Interfaces, 2015, 7, 9831–9840.

11 C. Shuai, G. Liu, Y. Yang, F. Qi, S. Peng, W. Yang, C. He, G. Wang and G. Qian, Nano Energy, 2020, 74, 104825.

12 Y. Mao, P. Zhao, G. McConohy, H. Yang, Y. Tong and X. Wang, Adv. Energy Mater., 2014, 4, 1–7.

13 L. Lu, W. Ding, J. Liu and B. Yang, Nano Energy, 2020, 78, 105251.

14 C. Li, W. Luo, X. Liu, D. Xu and K. He, Nanomaterials, 2016, 6, 1–9.

15 M. M. Abolhasani, K. Shirvanimoghaddam and M. Naebe, Compos. Sci. Technol., 2017, 138, 49–56.

16 B. Dudem, D. H. Kim, L. K. Bharat and J. S. Yu, Appl. Energy, 2018, 230, 865–874.

17 A. Sultana, M. M. Alam, P. Sadhukhan, U. K. Ghorai, S. Das, T. R. Middya and D. Mandal Nano Energy, 2018, 49, 380–392.

18 R. S. Sabry and A. D. Hussein, Mater. Res. Express, 2019, 6, 0–9.

19 U. Yaqoob, A. S. M. I. Uddin and G. S. Chung, Appl. Surf. Sci., 2017, 405, 420–426.